



Discontinuities-Driven Slope Stability Assessment and Mineralogical Studies Along Mughal Road, Jammu and Kashmir, India

R. Ingale¹ · Suhail Salroo¹ · B. K. Pandey²

Received: 7 July 2023 / Accepted: 8 December 2023 / Published online: 10 January 2024
© The Author(s), under exclusive licence to Springer Nature Switzerland AG 2024

Abstract

In contrast to their serenity, the roads cut through the Himalayas pose a significant threat to life and property, owing to their geomorphology, lithology, and status of discontinuities. The demarcation of unstable stretches along these roads through different geoenvironmental approaches is a valuable tool to mitigate the risks caused by these failures. The present research aims at assessing the stability of rock slopes and delineates the failure-susceptible/unstable slopes along the Mughal Road in the Srinagar district of Jammu and Kashmir, administered by India. The Mughal Road falls under a high-risk seismic zone (Zone-IV). The study employs different conventional and numerical geoenvironmental approaches to correlate the failure potential with the orientation of discontinuities and slope directions. The rock mass rating (basic) and Geological Strength Index (visual and quantified) have been utilized in the present study to determine the strength of the rock mass. Further, the discrete and continuous slope mass rating coupled with kinematic analysis and stereographic projections were adopted to assess the slope stability and identify the favorable discontinuity orientation for a particular type of failure. Eight sites along the study area were selected for the analysis, which was found to be partially stable to completely unstable. The seismic slope stability analysis is evaluated through pseudo-static analysis using Slope/W Software. Further, the mineralogical investigation studies used the X-ray diffraction method to support the analysis. The proposed framework for the analysis of the stability of slopes is a promising approach to capturing the real-time status and helps prevent failures.

Keywords Rock slope · Slope stability · Static analysis · Kinematic analysis · Pseudo-static analysis

Introduction

Slope failures are considered to be among the highly calamitous and most fatal types of natural hazard [1, 2]. They are associated with a quick drawdown of geo-materials which may be rocks, soils, debris, etc. [3]. Slope failure may be attributed to the basic strength criterion as, whenever the stresses accumulate, they surpass the strength of the material, and failure occurs. Several factors are triggering elements for slope failure, both natural and anthropogenic [4, 5]. Natural factors include topography, heavy precipitation,

seismic disturbances, neotectonic activities foliations, faults, schistosity, compositional banding, etc., while anthropogenic factors involve deforestation, urbanization, construction in the hilly areas, over-exploitation of natural vegetation, etc. [6]. Consequently, the slope failures along the Himalayan highways are rapidly increasing and hence pose a significant threat to the locals and commuters regarding loss of lives and properties [7]. Climate variation and weather conditions such as rainfall, temperature variation, freezing, and thawing action play a significant role in slope failures [8]. Considering the lethality of the slope failures and their impact on the socio-economic and environmental parameters, researchers and experts have always been called upon to analyze, assess and predict the behavior of given slopes under a different set of disturbing factors to provide remedial and mitigation measures [8, 9]. Researchers have given several methods to analyze the slopes (rock slopes, soil slopes and rock–soil mixed slopes), ranging from simplistic approaches to more complex and sophisticated methods [4]. Rock mass generally consists of two distinct constituents: Intact rock and

✉ R. Ingale
ritesh.ingale@nitsri.ac.in

¹ Department of Civil Engineering, National Institute of Technology Srinagar, Srinagar, Jammu and Kashmir (UT) 190006, India

² Department of Civil Engineering, Guru Ghasidas Vishwavidyalaya, Bilaspur, Bilaspur, Chhattisgarh 495009, India

Discontinuity (rendered as the plane of weakness). The mechanical aspect of the rock mass along which the tensile strength of the rock mass is zero is discontinuity. To evaluate the stability of rock slopes, conventional approaches employ limit equilibrium and kinematic analyses [10]. Numerical modeling techniques utilized to assess the rock slope stability are categorized as continuum, discontinuum, and hybrid. The continuum modeling comprises of finite element method (FEM) and finite difference method (FDM), which are the most popular among the three categories and considered the best-fit method for analyzing intact rock and highly fractured or disjointed rock mass [11]. Even if the stability of rock slopes is generally governed by the orientation, condition, and spatial distribution of discontinuities, it is practical to acknowledge the grade of the rock slope concerning an established on-site geological and structural framework [12]. In this regard, several geomechanical grading systems from time to time have been put forth in the concerned literature based on site-specific inputs and are accepted globally. The important conventional methods which are globally acknowledged include Rock Quality Designation (RQD), Rock Mass Rating (RMR) [13, 14], Rock Mass Strength (RMS) [15], Tunnelling Quality Index (Q-System) [16], Discrete Slope Mass Rating (DSMR) [17], Geological Strength Index (GSI) [18], Rock Mass Index (RMI) [19], Slope Stability Probability Classification (SSPC) [20, 21], and Continuous Slope Mass Rating (CoSMR) [22]. For elementary assessment of stability conditions of rock slopes, these classification systems have been considered effective and reliable tools [23]. Due to technological advancements, conventional methods are usually coupled with finite element methods (i.e., integrated analysis) to assess slope stability [4]. The generalized Hoek–Brown criterion is generally contemplated and applied in Shear Strength Reduction (SSR) analysis [24]. The SSR implies a systematic reduction in the material's shear strength to the extent that failure occurs. The SSR analysis produces the Stress Reduction Factor (SRF), which is portrayed as the ultimate factor of the safety of the material [24, 25].

Lesser Himalayas are considered the young, dynamic, and vibrant range of mountains continuously going through some tectonic disturbances. These tectonic disturbances, in conjunction with climatic factors such as rainfall, snowfall, freezing and thawing, avalanches and the topography (steep slopes, narrow gorges, etc.) of mountains, act as driving forces for slope failures [26]. Even though the Himalayas are prone to slope failures, these are enhanced by anthropogenic activities such as urbanization and other developments. These factors and development work along the rugged-terrain topographies, especially the Highway Development program, disturbs the in-situ equilibrium states of slopes, the consequence being enhanced and large-scale slope failure occurs [27].

The research carried out herein presents the integrated slope stability assessment of eight slopes along the Mughal Road (Pir-Panjal range of lesser Himalayas) initially using conventional methods such as RMR, SMR, Kinematic analysis using DIPS software [28, 29] and further GSI augmented with a limit equilibrium based static and pseudo-static analysis using Geo-Studio. The comparative analysis of the methods adopted has been presented in the study. Finally, the mineralogical studies using the X-ray diffraction technique (XRD) have been worked out to support the overall analysis.

Study Area Description

The Himalayan Mountain range presents fascinating and alluring geological attributes. Its rugged topography results from a strike between the Eurasian Plate (EP) and the Indian Plate (IP). The Himalayas have five structural units with different properties [30]: Sub-Himalaya, Lesser-Himalaya/Lower-Himalaya, Great/High-Himalaya, Tethys/Tibetan Himalaya, and Indus-Tsangpo. The Lesser Himalayan (young mountain chain) represents a sub-unit of the Himalayan orogeny that evolved from the rift between the Tibetan and the Indian lithospheric plates 50 Mega-annum ago.

The area under consideration in this study appertains to the road-cut slopes along the Mughal Road, which lies in the largest range of lesser Himalayas—the Pir-Panjal (local: *Peer-Panchaal*). The road is quasi-parallel to the main tributary of the river Rambi-ara. The Mughal Road (also called Imperial Road or Namak Road) is one of the critical interstate highways in the union territory of Jammu and Kashmir that connects National Highways NH-444 and NH-144. The road extends from Shopian (a hilly district in Kashmir valley) to Baffiaz (a small town in the Poonch district of Jammu province) and reduces the distance between the two localities by more than four times that is from 365 miles to a mere 78 miles. It passes through the largest range of lesser Himalayas—the Pir-Panjal range with an average elevation between 3000 and 3500 m above mean sea level.

The Pir-Panjal's climate is close to the Maritime Snow Climate, portrayed by mild to moderate temperatures and heavy snowfall with a characteristic feature of deep snow cover. It is important to mention here that, the places through which the road passes are Shopian, Heerpora, Dhobijan, Sathren, Zaznaar, Ali-abaad, Lal-Ghulam, and Peer ki Gali on the Kashmir side, while Chatta-Pani, Poushana, Chandimarh, Behram-Gali, and Baffiaz on Jammu side. Eight locations from the Kashmir side have been analyzed in the present study, shown in Fig. 1.

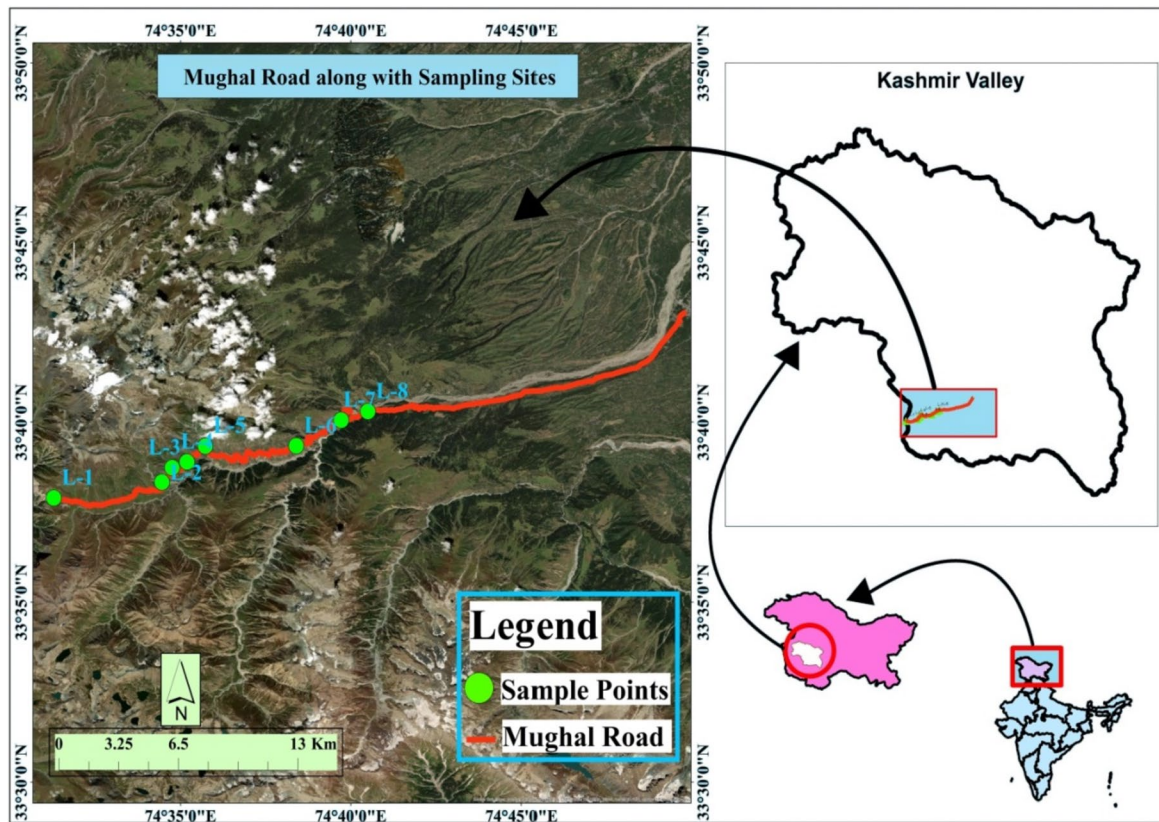


Fig. 1 Study area along with sampling sites (Mughal Road, J&K)

Geological and Structural Details

Along the study area, the main lithological units are Tuffaceous and Clastic Sediment of Nishat-bagh Formation (Lower-Permian), Pebbly Slate and Quartz Arenite Conglomerate of Agglomeratic Slates (Lower-Permian), Schistose, flaggy Quartzite and Volcanics of Kalmund Formation (Dogra Group) and Sand, Conglomerate and Lignite of Hirpur Formation (Karewa Group, Middle Miocene to lower Pleistocene). The area is structurally delineated by Panjal Thrust (PT), regional Main Boundary Thrust (MBT), Neo-tectonic thrust, and some local faults like Chandimarh, Beharamgalli, and Dugrian faults [31].

Mineralogical Studies Using X-Ray Diffraction

The mineralogical analysis in the present study was performed using XRD (X-ray Diffraction Test). The XRD test was performed within the Bragg's angles 0° – 80° (2θ), using copper (Cu) radiations, at voltage 45 kV, 40 mA beam current on Rigaku Smart Lab X-ray Diffractometer performed at Central Research Facility Centre (CRFC) of National Institute of Technology, Srinagar. The obtained peaks from XRD were matched with the ICDD PDF card (International Centre

for Diffraction Data Powder Diffraction File Card) for analyzing the mineral. The XRD analysis of the samples showed that the commonly found minerals along the study area were Quartz (SiO_2), Muscovite (hydrated phyllo-silicate of potassium and aluminum, $(\text{KF})_2(\text{Al}_2\text{O}_3)(\text{SiO}_2)_6(\text{H}_2\text{O})$), Albite ($\text{NaAlSi}_3\text{O}_8$), Calcite (CaCO_3), Haematite (Fe_2O_3), Cobalt Dysprosium Germanide (Co_2DyGe_2), and Dysprosium Copper Germanide (DyCuGe). Further, the X-ray diffraction analysis of eight sites from the study area is presented in Fig. 2. The periodicity in the atomic structure (orderly placement of atoms) causes diffraction, i.e., constructive interference, and hence a strong relation exists between periodicity and diffraction. For shorter periodicity, higher diffraction angles are observed [32].

Methods and Results

Rock Mass Characterization

The site under consideration was explored through several visits to the study area. The methodology for assessing slope stability involves using a scan-line survey for creating linear paths (scan lines) on a slope of interest and systematically

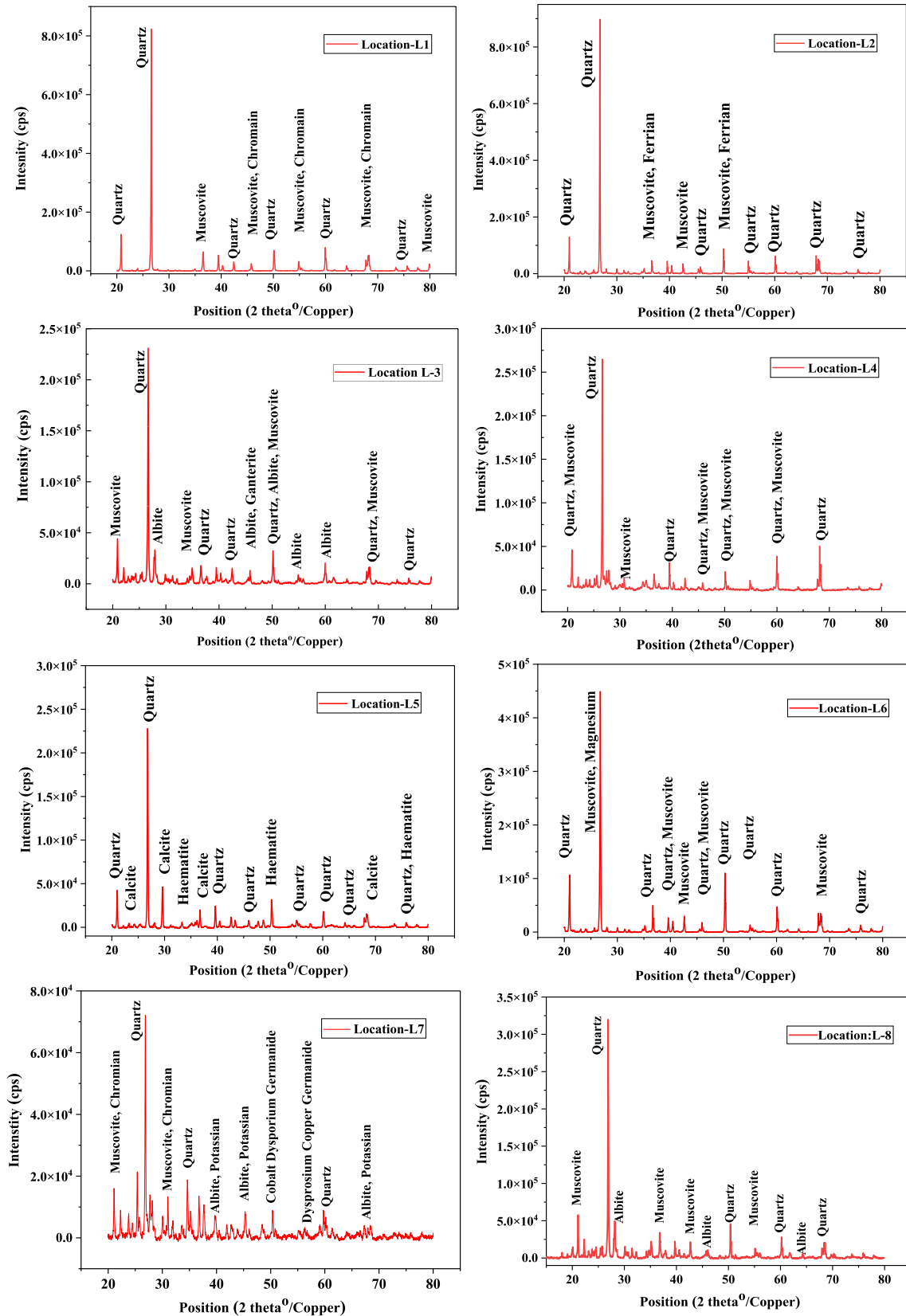


Fig. 2 XRD analysis results for eight sights along Mughal Road

collecting geological, geotechnical, and topographic data along these lines. This process begins with defining survey objectives and selecting appropriate sites. Surveying equipment, including instruments for precise measurements and safety gear, is then gathered. Scan lines are established, perpendicular to slope contours, and marked with precise starting and ending points. Data collection along these lines includes recording geological features, measuring geotechnical properties, documenting topography, and visually inspecting for signs of instability. Safety precautions are paramount. Data analysis involves stability assessments, identifying potential failure mechanisms, and considering external factors. Adopting the Scan-Line survey, preliminary slope dimensions and discontinuity data as a dip, dip direction, persistence, spacing, and groundwater condition data were captured from the eight locations of the Mughal Road as indicated earlier (Refer to Fig. 1). The weathering class of the slopes has been assessed through various techniques including visual inspection, scraping the rock material with hands, and noting the colour variations in the rock mass and

sound of the rock mass under the strike of the geological hammer.

Rock-quality designation (RQD) determines roughly the degree of fractures in a rock mass. RQD is expressed as the percentage of the drill core in lengths of 10 cm or more. A high value of RQD indicates high-quality rock mass and vice-versa. The Rock Quality Designation (RQD) is empirically estimated with the help of volumetric joint count J_v for road-cut sections as expressed in the following equation:

$$RQD = 115 - 3.3 J_v = 100 \quad \text{if } J_v < 4.5. \tag{1}$$

A minimum value of RQD shall be reported as ten even if it is zero [33]. Further, the volumetric joint count (J_v) implies the joint number in 1 metric cube of rock mass [19]. Empirically, J_v is expressed as per the following equation:

$$J_v = \frac{1}{S_1} + \frac{1}{S_2} + \dots + \frac{1}{S_n}. \tag{2}$$

The S_1 , S_2 , and S_n are the mean joint set spacing. The statistical attributes of the joint data are presented in Table 1.

Table 1 Statistical attributes of discontinuities at various sites along Mughal Road

Statistical attributes of discontinuities at various sites along Mughal Road									
Site	Joint set	Statistical attributes of joint spacing (m)			(J_v) Joints/m ³	RQD (%)	Block index	V_b (m ³)	Description
		Max	Min	Mean					
L-1	JS-1	0.95	0.2	0.69	4.86	98.95	0.62	0.31	Medium sized blocks
	JS-2	0.9	0.25	0.64					
	JS-3	0.95	0.1	0.54					
L-2	JS-1	0.9	0.25	0.66	4.67	99.57	0.66	0.35	Medium sized blocks
	JS-2	0.8	0.2	0.52					
	JS-3	0.85	0.1	0.81					
L-3	JS-1	0.78	0.25	0.50	6.19	89.5	0.49	0.15	Medium sized blocks
	JS-2	0.76	0.2	0.41					
	JS-3	0.98	0.1	0.57					
L-4	JS-1	0.87	0.1	0.50	6.56	88.32	0.46	0.13	Medium sized blocks
	JS-2	0.55	0.05	0.39					
	JS-3	0.8	0.08	0.50					
L-5	JS-1	0.7	0.09	0.42	10.55	75.17	0.30	0.03	Small blocks
	JS-2	0.4	0.08	0.24					
	JS-3	0.65	0.05	0.25					
L-6	JS-1	0.5	0.05	0.24	14.59	62.19	0.21	0.01	Small blocks
	JS-2	0.35	0.06	0.22					
	JS-3	0.27	0.06	0.17					
L-7	JS-1	0.46	0.05	0.24	17.08	53.62	0.18	0.01	Small blocks
	JS-2	0.32	0.06	0.15					
	JS-3	0.35	0.04	0.16					
L-8	JS-1	0.9	0.25	0.55	6.67	88.14	0.52	0.12	Medium sized blocks
	JS-2	1.2	0.25	0.71					
	JS-3	0.5	0.04	0.29					

The block size varies along the study area from small to medium-sized blocks, with block volume varying between 0.01 and 0.35 m³.

Rock Mass Rating (RMR)

Rock Mass Rating (RMR), introduced by Bieniawski [13, 14], is colossally used in many rock engineering projects related to slope stability, underground excavations, mining, tunnelling, and dams. The RMR proposed by Bieniawski [13] was updated by many researchers on experience gained through intensive fieldwork in the following years. The developed RMR system uses six parameters, namely, Uniaxial Compressive Strength (UCS) of rock material, Rock Quality Designation (RQD), features of discontinuities (i.e., Spacing, Condition, and Orientation), and Groundwater conditions. However, in RMR basic (RMR_{basic}), five parameters are used to study the rock mass, and the orientation of discontinuities needs to be considered. An indigenously fabricated low-cost cylindrical core cutter of NX, shown in, Fig. 3, has been used to extract the test specimens for UCS [20].

Geological Strength Index (GSI)

A rock mass's deformation and strength properties are estimated by the Hoek–Brown criterion using the Geological Strength Index (GSI), as introduced by Hoek and Brown [15] and later modified by Russo and Hormazabal [21]. The

Hoek–Brown model assumes that the rock mass behaves as an isotropic, homogeneous material with uniform properties. Rock masses often contain geological features such as joints, faults, bedding planes, and shear zones that can significantly affect their behavior. These discontinuities are not explicitly considered in the Hoek–Brown model. The GSI characterizes the blocky rock mass based on visual inspection of the outcrop, jointing conditions, and interlocking. The GSI value ranges from 0 to 100. The rock mass classification and characterization as per GSI are uncomplicated as it is based upon the visible perception of the rock-mass structure in terms of top surface properties of the joints indicated by joint alteration and roughness, and blockiness of the surface.

To simplify the procedure further, Hoek et al. and other researchers [18, 42] have suggested a more simplistic approach to calculate the GSI using RQD and the condition of joints, which is as follows:

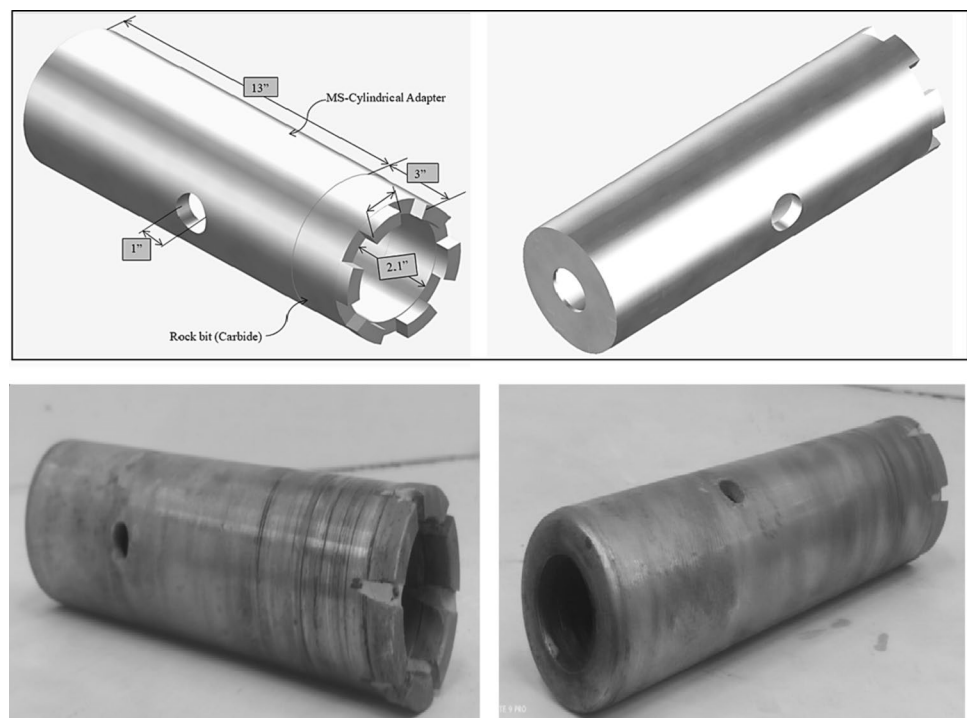
$$GSI = \left(\frac{RQD}{2} \right) + (1.5 \times J_{cond89}), \quad (3)$$

where

$$J_{COND89} = 35 \times \left[\frac{J_r/J_a}{1 + J_r/J_a} \right]. \quad (4)$$

J_r is the joint roughness rating, and J_a is the joint alteration rating. This is referred to as GSI quantification [42]. The RMR_{basic} and GSI values along the study area are presented

Fig. 3 Isometric and fabricated views of rock core cutter



in Table 2. The RMR for the sites varies from 44 to 78, representing fair to good rock, and GSI varies between 40 and 85.

Slope Characterization

Assessment Through Slope Mass Rating (SMR)

Slope mass rating (SMR) represents the rock slope characterization scheme introduced by Manuel Romana in 1985 [44] to characterize and assess the slope in terms of susceptibility to various failures. Later, Anbalagan [28] added the adjustment ratings for the wedge failure. This system incorporates an RMR_{basic} scheme in conjunction with the parameters defined by the orientation of the joints [44, 45]. The equation for SMR:

$$SMR = RMR_b + (F_1 \times F_2 \times F_3) + F_4. \tag{5}$$

RMR_b is the basic RMR considering the five parameters discussed above. The F_1 depends on parallelism between the slope and the discontinuity; F_2 depends on the dip of discontinuity; F_3 depends on the relationship between the discontinuity dip and slope inclination; and F_4 depends on the excavation method used. Tomás et al. [22] described alternative continuous functions for calculating F_1 , F_2 , and F_3 correction parameters. This method is referred to as Continuous Slope Mass rating (CSMR). These continuous functions vary from discrete functions by less than 7–8 points and thus retard the subjective interpretations significantly. Withal, the proposed continuous functions for SMR alteration factors ambiguity generated due to the rounding off the discrete factors. The SMR, both discrete and continuous for the selected slopes, is presented in Table 3. The SMR table indicates that the stability class along the study area varies from Class-II (Stable) to Class-V (Completely unstable). Also, the probability of failure ranging from 0 to 0.9 represents the stability classes for respective sites [44, 45].

Assessment Using Kinematic Method

The kinematic analysis of rock mass is a function of discontinuity attitudes/orientation. Kinematic analysis calculates if the blocks or rock masses move along geologic features/attitudes and slide out of the slope [34]. The following three types of failure modes have broadly been identified in rock engineering throughout the years of research and experience: plane failure, wedge failure, and toppling [35]. Through scan-line mapping, the discontinuity data have been collected from the sites. The kinematic analysis has been performed using DIPS software using stereographic projections (Schmidt’s equal angle method).

Table 2 RMR and GSI for selected slopes

Site	UCS	RQD	Joint condition		Joint spacing					RMR basic	Description	GSI	
			Length	Aperture	Rough	Infilling	Weathering	Visual	Quantified				
L-1	12	20	2	4	4	3	3	15	15	78	II/Good rock	80	85.02
L-2	7	20	1	0	1	0	1	15	10	55	III/Fair rock	65	68.29
L-3	7	17	2	1	1	4	5	10	7	54	III/Fair rock	60	62.25
L-4	7	17	2	1	1	2	3	9	7	49	III/Fair rock	55	52.45
L-5	7	17	1	0	1	0	3	10	7	46	III/Fair rock	55	51.9
L-6	7	13	1	1	3	2	5	10	7	49	III/Fair rock	50	45.41
L-7	7	13	2	0	1	6	1	10	4	44	III/Fair rock	40	44.31
L-6	7	17	4	2	5	2	5	10	4	56	III/Fair rock	70	66.57

Table 3 SMR indices (discrete and continuous) and stability class thereof

Site	Joint set	RMR basic	Failure observed	$F_1 * F_2 * F_3$		F_4	SMR		Class of stability	Failure probability
				Romana discrete	Tomas continuous		Dis.	Cont.		
L-1	JS-1	78	P/W	-1	-2	0	77	76	II/S	0.2
	JS-2	78		0	0		78	78	II/S	0.2
	JS-3	78		-24	-21		54	57	III/PS	0.4
L-2	JS-1	55	P/W	-24	-34	0	31	21	IV/U	0.6
	JS-2	55	Toppling	0	0		55	55	II/S	0.2
	JS-3	55	P/W	-8	-9		47	46	III/PS	0.4
L-3	JS-1	54	Toppling	-18	-19	0	36	35	IV/U	0.6
	JS-2	54		-4	-6		50	48	II/S	0.2
	JS-3	54		-4	-5		50	49	III/PS	0.4
L-4	JS-1	50	Toppling	-18	-16	0	32	34	IV/U	0.6
	JS-2	50	P/W	-4	-3		46	47	III/PS	0.2
	JS-3	50	P/W	-4	-3		46	47	III/PS	0.4
L-5	JS-1	46	P/W	-42	-31	0	4	15	V/CU	0.9
	JS-2	46	Toppling	0	0		46	46	III/PS	0.2
	JS-3	46	P/W	0	0		46	46	III/PS	0.4
L-6	JS-1	49	Toppling	-1	0	0	48	49	III/PS	0.2
	JS-2	49	P/W	0	0		49	49	III/PS	0.2
	JS-3	49	P/W	-8	-16		41	33	III-IV	0.4
L-7	JS-1	44	P/W	-4	-4	0	40	40	IV/U	0.6
	JS-2	44	Toppling	-25	-25		19	19	V/CU	0.9
	JS-3	44	P/W	0	0		44	44	III/PS	0.4
L-8	JS-1	56	P/W	-21	-23	0	35	33	IV/U	0.6
	JS-2	56	Toppling	-8	-10		48	46	III/PS	0.2
	JS-3	56	P/W	-8	-10		48	46	III/PS	0.2

Planar failures represent the movement of sliding on a unique and distinct surface that nearly approximates a plane. Hoek et al. [36] and later Hoek and Brown [15] set up the conditions for the planar failure viz; The dip of the discontinuity must lie within 20 degrees of the dip of slope face, shall not exceed the dip of the slope face, shall not be less than the angle of friction of the surface. Also, the sideward extent of the failure surface shall be defined either by lateral release surfaces or by a convex slope shape intersected by discontinuity.

Wedge failures in a rock mass occur when a slide of rock mass exists along the two intersecting joints dipping out of the excavated slope at an angle concerning the cut slope, forming a wedge-shaped feature. Primarily the formation and hence occurrence of these wedge failures are functions of rock-mass structure and lithology [1, 36]. Limestones, shale, clay stones, and fine-bedded siltstones are more inclined to wedge failures than other rock types. The three essential structural conditions described for wedge failures by Hoek et al. [36] and can be summed up as follows: The trend of the line of intersection shall be

close to the dip of the slope face; the Plunge of the intersection line shall not be greater than the slope dip. The plunge of the intersection line shall not be less than the internal friction angle of the surface.

Toppling failures occur mostly in rock masses divided into slabs or columns (fragmentation). These fragments/fractures have a geological attitude such that they strike nearly parallel to the face of the slope and steeply dip into the slope face. Hoek et al. [36] and later Hoek and Bray [37] defined types of toppling failures, such as block toppling, flexural toppling, or a union of the above two types. These failure types in the study area are shown in Fig. 4.

The kinematic analysis is two-dimensional; hence it is presumed that zero-strength sideward release surfaces are there or that the failure of rock mass is described in the plan by a convex slope [37]. The results from the kinematic analysis are tabulated in Table 4, and corresponding Stereonets are presented in Fig. 5. The kinematic analysis implies that the selected slopes along the study are susceptible to various slope failures with varying degrees of severity.

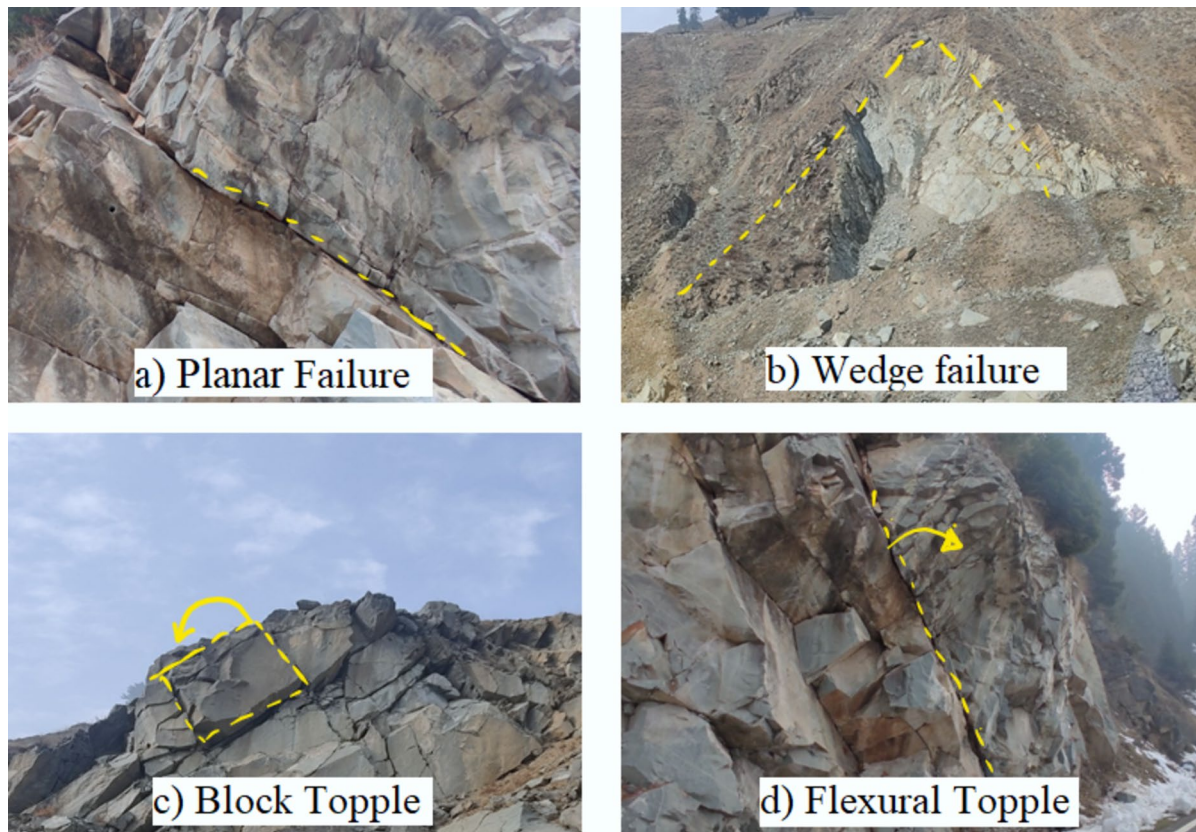


Fig. 4 Four types of failure identified along the study area

Table 4 Kinematic analysis results using DIPS software

Site	Slope Dip°	Critical intersection %age for following failures					
		Wedge	Planar	Direct toppling	Flexural toppling	Oblique toppling	Base plane toppling
L-1	65	28.65	6.06	33.33	0.00	1.90	33.33
L-2	77	14.77	16.67	3.22	0.00	0.00	51.52
L-3	72	2.08	0.00	12.31	27.27	0.19	0
L-4	76	4.55	3.03	2.85	24.24	0.57	39.39
L-5	62	17.70	26.67	1.61	0.00	1.61	20.00
L-6	68	34.05	0.00	1.61	0.00	1.29	16.13
L-7	72	0.00	9.38	3.02	31.25	3.47	34.38
L-8	65	5.29	6.25	9.38	34.38	1.16	34.38

Limit Equilibrium Methods

The limit equilibrium implies the condition where the driving and resisting forces are equal (limit state status), and the corresponding safety factor equals unity. This condition implies that the block under consideration is on the verge of failure; even a slight disturbance to the equilibrium conditions can set the block to tumble/slide [38]. The basic methodology involved in the limit equilibrium analysis includes the calculation of the factor of safety by giving

the driving and the resisting forces as inputs to the rock mass. For an FOS greater than unity, the block under consideration is safe for a given set of inputs, while in other cases, the block is not safe. This method divides the material overlying the assumed slip surface vertical slices. The LE analysis has been assessed using SLOPE/W software using the Morgenstern–Price method using Hoek–Brown failure criteria. This method was chosen since it is an accurate procedure applicable to virtually all slope geometries and soil profiles, a rigorous, well-established, complete

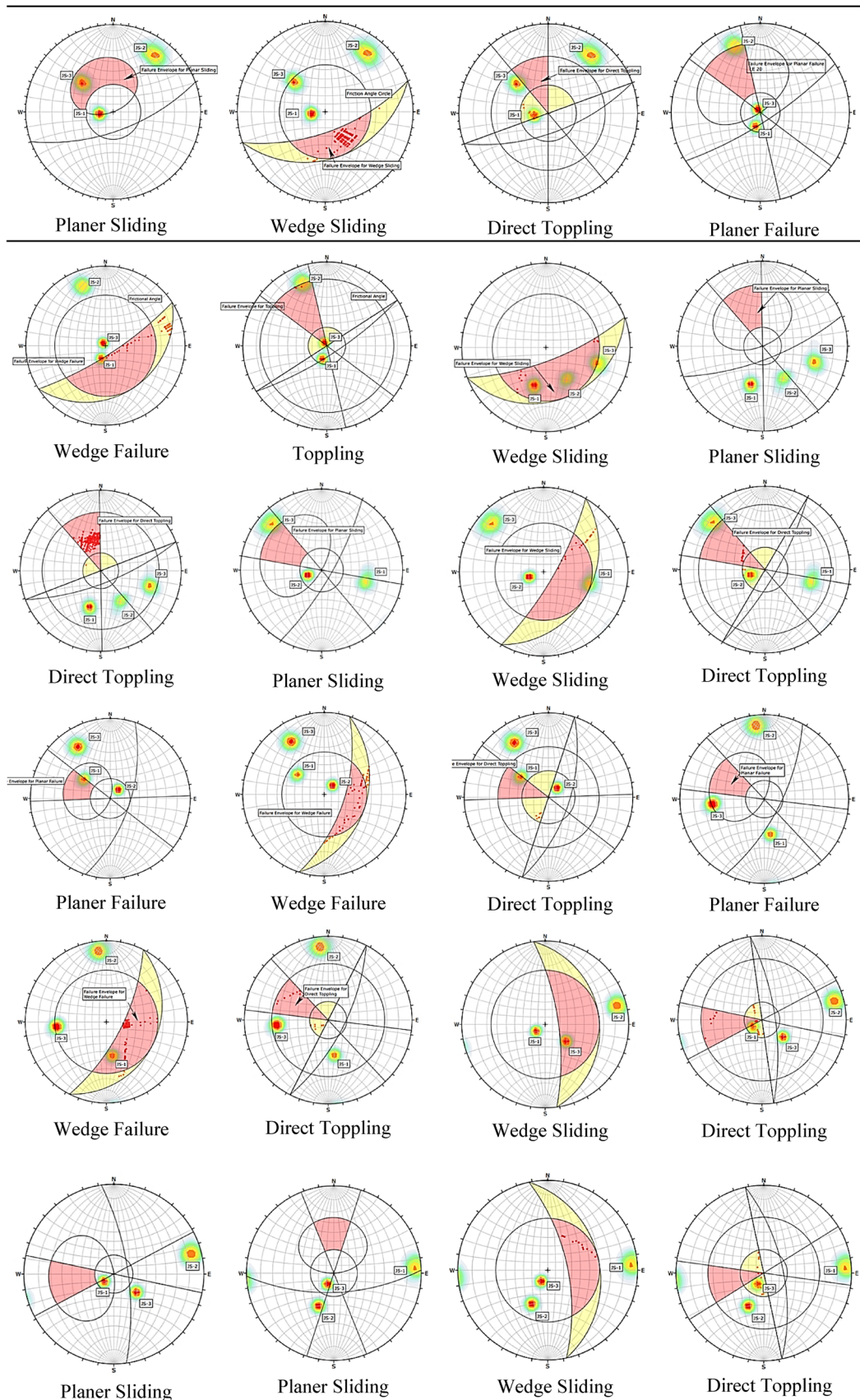


Fig. 5 Stereonets for different failure modes along selected slopes

equilibrium procedure. Further, it helps in more reliable and robust designs of slopes.

The modeling procedure was validated with the study of Rajhans et al. [39], where the stability of the mine dumps was determined after improving the dump using soil nails. The Geo-studio Slope/w was also used in the referred study, in which the Morgenstern–Price approach is used for the analysis, with the constant interslice force function, and the slip surfaces are constructed using an entry–exit procedure. The model dimensions and material properties were directly taken from the referred study. As seen from Fig. 6, the obtained FOS from the present study is in good agreement with the referred study of Rajhans et al. [39]. This shows that the adopted modeling procedure can be applied to simulate the problem at hand.

The Mohr–Coulomb failure criterion can be expressed for the rock mass as follows:

$$\tau = C' + \sigma'_n \times \tan(\phi'), \tag{6}$$

where C' is the effective cohesion and ϕ' is the effective friction angle. The Mohr–Coulomb failure criterion parameters are estimated empirically computed using the following equations [37, 40]:

$$\phi' = \sin^{-1} \left[\frac{6 \times a \times m_b \times (s + m_b \sigma'_{3n})^{a-1}}{2(1+a)(2+a) + 6 \times a \times m_b \times (s + m_b \sigma'_{3n})^{a-1}} \right] \tag{7}$$

and

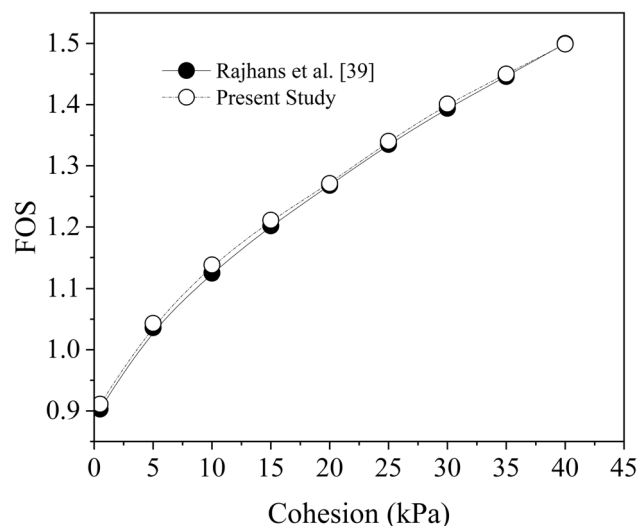


Fig. 6 The validation of present study with the Rajhans et al. [39]

$$C' = \frac{\sigma_{ci} [(1 + 2a)s + (1 - a)m_b \sigma'_{3n}] \times (s + m_b \sigma'_{3n})^{a-1}}{(1 + a)(2 + a) \times \sqrt{1 + \frac{6 \times a \times m_b \times (s + m_b \sigma'_{3n})^{a-1}}{(1+a)(2+a)}}}, \tag{8}$$

where

$$\sigma'_{3n} = \left(\sigma'_{3\max} / \text{UCS} \right). \tag{9}$$

In the case of slopes, the relation between $\sigma'_{3\max}$ and σ'_{cm} can be found using the following equation [18]:

$$\sigma'_{3\max} = \sigma'_{cm} \times 0.72 \times \left(\frac{\sigma'_{cm}}{\gamma \times H} \right)^{-0.91}, \tag{10}$$

where γ represents the rock-mass unit weight; H represents slope height and σ'_{cm} compressive rock mass strength. Hoek et al. [18] produced the generalized Hoek–Brown failure criterion for rock masses and is given by:

$$\sigma'_1 = \sigma'_3 + \left\{ \text{UCS} \times \left(m_b \times \frac{\sigma'_3}{\text{UCS}} + s \right)^a \right\}, \tag{11}$$

where σ'_1 and σ'_3 represent the maximum and minimum effective principal stresses; m_b represents the Hoek–Brown constant for rock mass; s and a are the constants that are functions of rock mass characteristics, and UCS represents the uniaxial compressive strength of rock mass. The deformation properties of rock mass generally include the modulus of deformation and the Poisson’s ratio (μ). Following are the methods to compute deformation modulus:

(i)(i)(i) The deformation modulus for $\text{UCS} \leq 100$ MPa, is given by:

$$E_m = \left(1 - \frac{D}{2} \right) \times \sqrt{\frac{\sigma_{ci}}{100}} \times 10^{\left(\frac{\text{GSI}-10}{40} \right)}. \tag{12}$$

(ii)(ii)(ii) For $\text{UCS} > 100$ MPa the value of E_m is given by:

$$E_m = \left(1 - \frac{D}{2} \right) \times 10^{\left(\frac{\text{GSI}-10}{40} \right)}. \tag{13}$$

A value of 0.3 for Poisson’s ratio has been judiciously chosen in the present study following Latha and Garaga [9]. The bulk and shear moduli (K_r and G_r , respectively) are computed by the following equation:

$$G_r = \frac{E_r}{2 \times (1 + \mu_r)}; \text{ and } K_r = \frac{E_r}{3 \times (1 - 2\mu_r)}. \tag{14}$$

The rock mass parameters are calculated using the above equations and are tabulated in Table 5. The cross-section

Table 5 Estimated Hoek–Brown and Mohr–Coulomb parameters

Site	GSI	m_i	m_b	s	a	σ_{ci} (MPa)	σ_{cm}' (MPa)	σ_{3max}' (MPa)	σ_{3m}' (MPa)	c' (MPa)	ϕ°	E_r (GPa)	K_r (GPa)	G_r (GPa)
L-1	85.02	25	11.4	0.08677	0.50	105.5	52.41	21.79	0.21	1.96	48.1	18.2	7.03	15.2
L-2	68.29	16	3.27	0.00674	0.50	71.4	17.48	14.57	0.20	0.46	37.9	13.3	5.13	11.1
L-3	62.25	15	2.90	0.00603	0.50	59.2	13.64	12.32	0.21	0.36	36.7	12.5	4.84	10.4
L-4	52.45	14	2.27	0.00346	0.51	56.7	11.37	14.98	0.26	0.37	32.6	9.44	3.63	7.87
L-5	51.9	14	1.96	0.00248	0.51	66.8	12.34	17.01	0.25	0.37	31.7	7.94	3.06	6.62
L-6	45.41	14	2.27	0.00346	0.51	55.1	11.05	14.83	0.27	0.36	32.4	9.44	3.63	7.87
L-7	44.31	13	1.76	0.00198	0.51	72.3	12.56	14.33	0.20	0.27	32.8	7.08	2.72	5.90
L-8	66.57	17	3.31	0.00674	0.50	76.7	18.88	11.80	0.15	0.37	40.4	13.3	5.13	11.1

of different study sites is shown in Fig. 7 (analyzed using Bhuvan 3D, Indian remote Sensing Satellites, ISRO, GoI).

landslide. However, the slope encountered in the present studies are generally steeper.

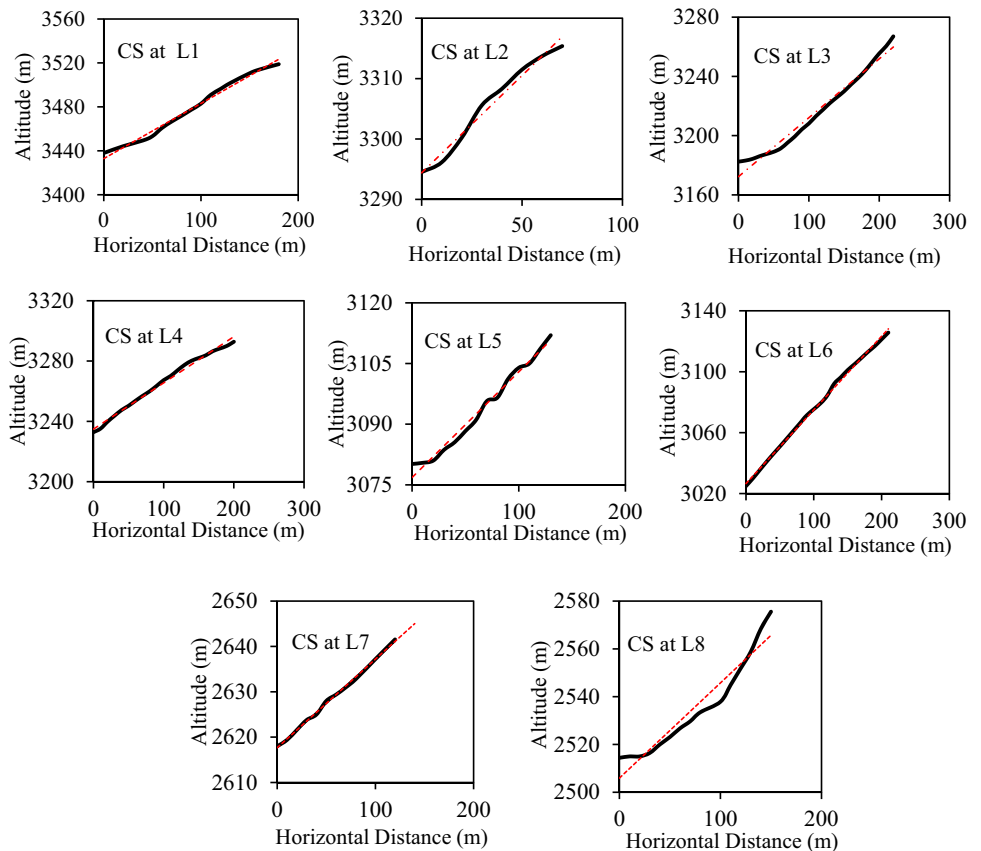
Assessment Using Mineral Composition

The pre-existing rock mass composition is consistent with the XRD analysis results. It reveals no expandable or clay minerals exists and major minerals are quartz and muscovite within the rock mass to allow the soil to slide. It is worth mentioning that, the clay forming minerals generally formed from the chemical weathering which may cause debris

Pseudo-static Analysis

The Pseudo-static analysis incorporates the imitation of the ground motion as the fixed static horizontal force which acts out of slope-face [41]. This methodology involves the effects caused due to the pseudo-static acceleration during an earthquake which generates the inertial forces, also called pseudo-forces, the magnitude of which is described as the product of seismic acceleration and the mass of rock

Fig. 7 Cross section of selected slopes along the study area



block under effect. The value of α_h (horizontal seismic coefficient) is generally taken as design Peak Ground Acceleration (PGA) expressed in terms of gravity acceleration. The resisting forces are reduced and driving forces are increased by horizontal seismic force while the vertical seismic force has the least significant effect on the stability analysis, hence usually neglected in the pseudo-static analysis. However, to get conservative results, the present study covers the effect of vertical acceleration as well.

Hence, the value of α_h shall be carefully and judiciously chosen. MCE (Most Credible Earthquake) data are generally reliable to choose the value of the horizontal coefficient. The study area is in a high-risk seismic zone and hence a value of 0.32 g following Metya et al. [42] has been chosen for the present study based on the previous history of the region. The vertical coefficient (α_v) has been taken as 0.667 times the α_h [42].

In present study, the pseudo-static analysis of the slopes under consideration has been done for two cases:

- (i) Considering both horizontal and vertical seismic accelerations; and
- (ii) Only horizontal seismic acceleration has been considered.

Pseudo-static analysis has been also worked out in SLOPE/W of Geo-Studio. The LE and Pseudo-static analysis results are interpreted in Fig. 8. The results obtained from limit equilibrium analysis and pseudo-static analysis using the Morgenstern–Price method considering Mohr–Coulomb and Hoek–Brown failure criteria are tabulated below in Table 6. The factor of safety varies from 0.4 to 0.8 under static loading while from 0.35 to 0.75 under pseudo-static loading.

Discussion and Analysis

Rock Mass Characterization

The fracture data or discontinuity data from the eight selected sites along the study area were collected from the site using scan-line mapping. The collected data include orientation, spacing, roughness, persistence, aperture, filling, seepage, number of sets, and block size. The relation between volumetric joint count and block volume, J_v and V_b , respectively, for the selected slopes, are shown in Fig. 9. J_v and V_b share a reciprocal relationship, i.e., for higher values of joints per volume, the block size is smaller. The inverse relationship between joint and block volumes originates from geometric and mechanical factors in rock slope analysis. Higher joint density increases joint volume but smaller intact rock blocks, influencing stability. Joints act

as stress concentrators, affecting load distribution, and shear strength. Block failures are common with low joint density, while joint-controlled failures often occur with high joint density. Slope angle and rock mass quality further influence this relationship. Field data from the selected slope suggest that the block size varies from small to medium size with medium to high volumetric joint count. The results from the statistical analysis showed that the selected sites along the study area contain three joint sets with varying degrees of block volume. These findings are attributed to the location and lithology of the area. The sites with smaller block sizes require a small triggering force to cause failure; hence it can be put forth that these sites are more susceptible to failure.

The RMR basic analysis showed the rock quality along the area varied from fair to good rock with basic RMR values varying between 40 and 80. While GSI values varied between 40 and 80. The variation of RMR and GSI along the study area is represented in Fig. 10. The variation of GSI-Visual and GSI quantified are presented in Fig. 11.

The visual GSI as put forth by Hoek et al. [15], based on visual inspection has been simplified and quantified by different workers. The above comparison shows the two aspects of GSI, i.e., visual, and quantified are in good agreement with each other concerning the numerical valuation.

Slope Characterization

Slope Mass Rating

Slope Mass Ratings both discrete and continuous put forward by Romana and Tomas, respectively, have been assessed for the slopes along the study area.

The SMR analysis procured that the slope mass varies from completely unstable to stable for different modes of failure with a probability of failure at some slopes as high as 0.9. The variation of CSMR along the different joint sets for selected slopes is shown in Fig. 12.

The slope mass rating indices put forth by Romana [17] and later Tomás et al. [22] differ from each other as the former has used discrete valuation while the latter has adopted continuous function. The discrete adjustment indices (F_1 , F_2 , and F_3) usually overestimate the toppling-related stability condition. Hence to resolve this over-conservative nature of discrete SMR systems [22], put forth the concept of continuous indices. The variation between DSMR and CSMR is depicted in Fig. 13.

Kinematic Analysis

The kinematic analysis of these slopes indicates a variety of slope failures along different orientations. The overall critical intersections for different modes of failure vary between 0 and 52%. The orientation of the joints along the study area

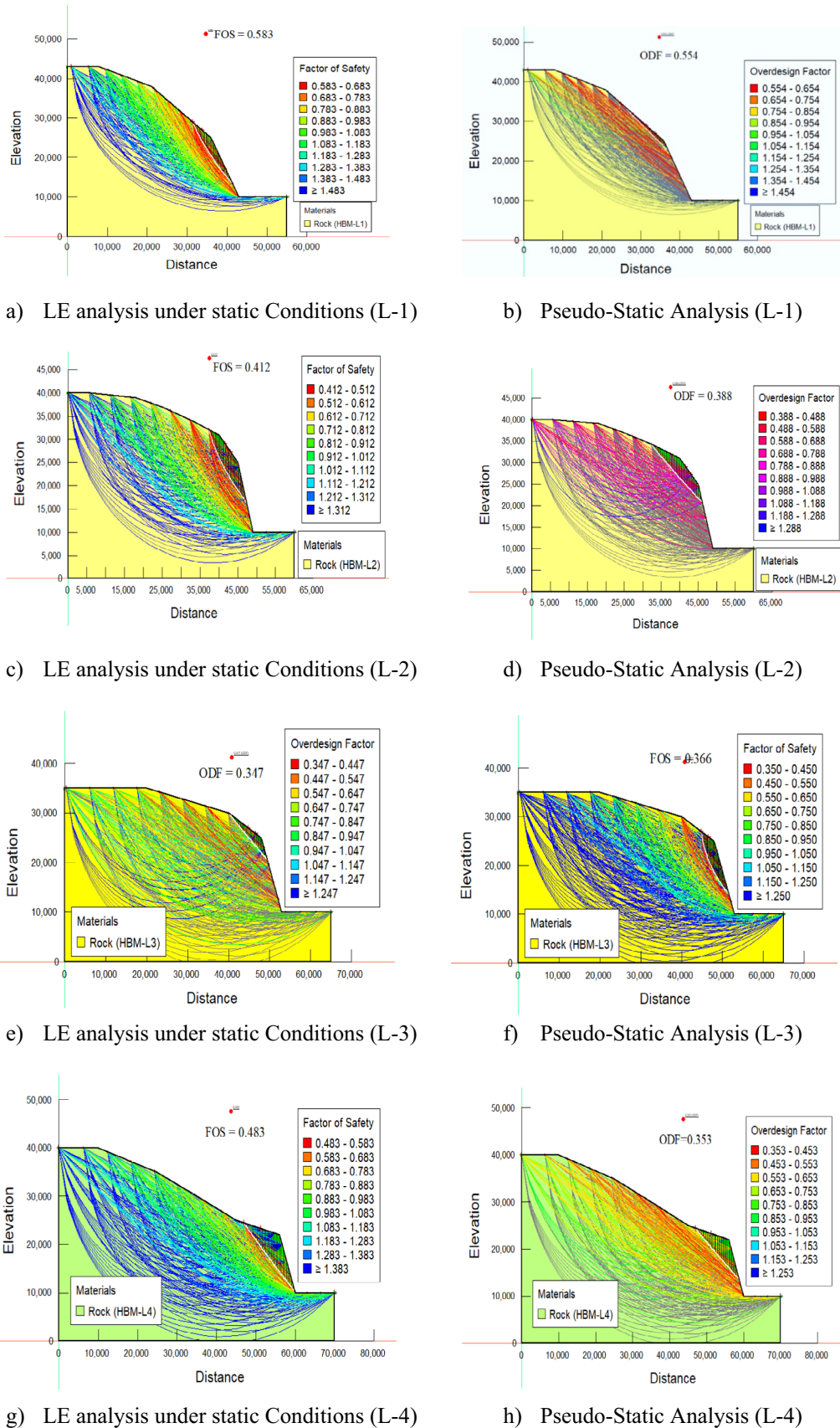
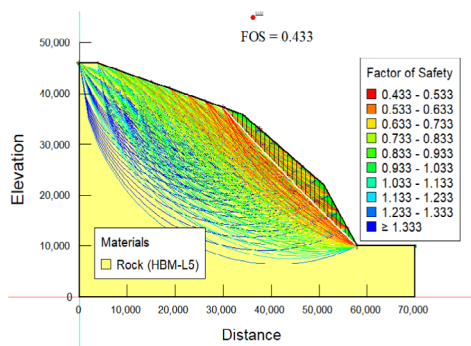
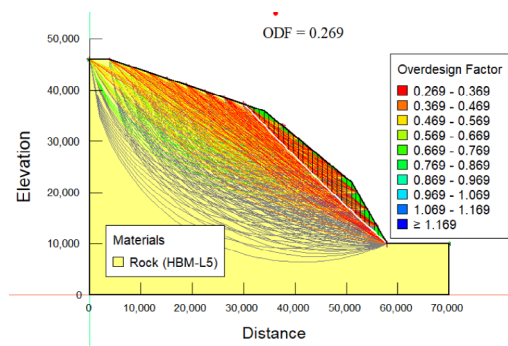


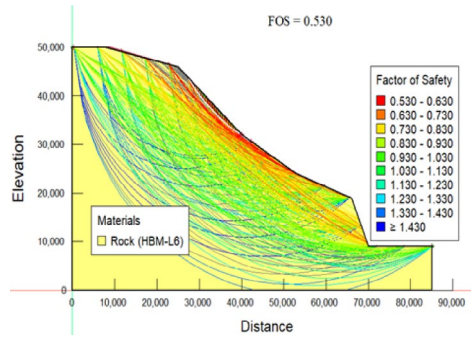
Fig. 8 Observed factor of safety for selected slopes under different conditions



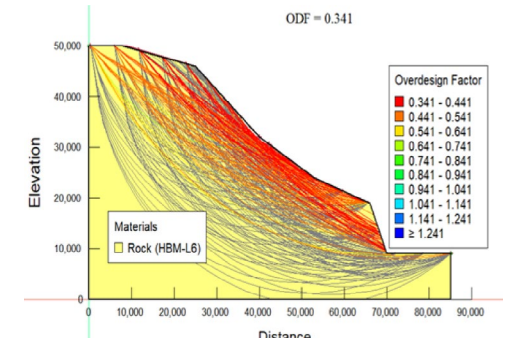
i) LE analysis under static Conditions (L-5)



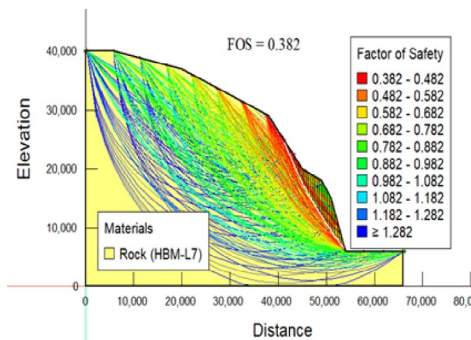
j) Pseudo-Static Analysis (L-5)



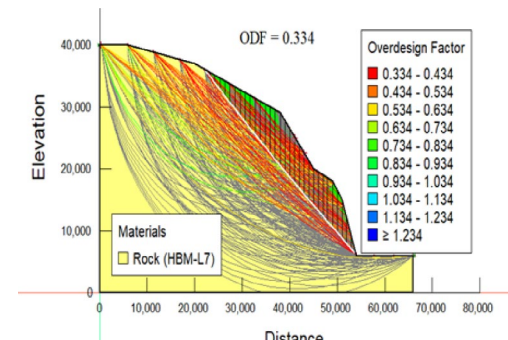
k) LE analysis under static Conditions (L-6)



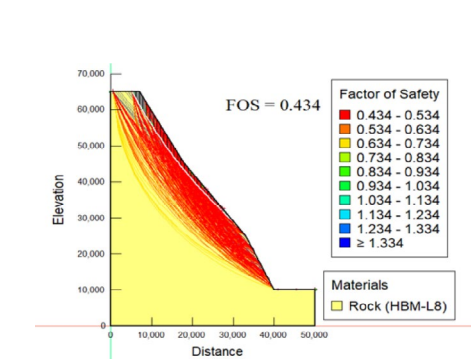
l) Pseudo-Static Analysis (L-6)



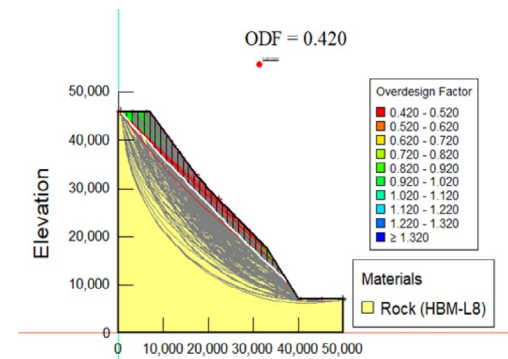
m) LE analysis under static Conditions (L-7)



n) Pseudo-Static Analysis (L-7)



o) LE analysis under static Conditions (L-8)



p) Pseudo-Static Analysis (L-8)

Fig. 8 (continued)

Table 6 LE analysis and pseudo-static analysis results

Site	RMR	GSI	UCS	Kinematic results	Factor of safety					
					Mohr–Coulomb			Hoek–Brown		
					Static	$\alpha_h=0.31, \alpha_v=0.11$	$\alpha_h=0.31, \alpha_v=0.0$	Static	$\alpha_h=0.31, \alpha_v=0.11$	$\alpha_h=0.31, \alpha_v=0.0$
L-1	78	85.02	105	Direct toppling	0.77	0.723	0.766	0.58	0.554	0.587
L-2	55	68.29	71.4	Base plane	0.5	0.524	0.525	0.41	0.388	0.396
L-3	54	62.25	59.2	Flexural toppling	0.47	0.467	0.494	0.37	0.347	0.369
L-4	49	52.45	56.7	Base plane	0.59	0.433	0.49	0.48	0.353	0.375
L-5	46	51.9	66.8	Planar	0.78	0.481	0.51	0.43	0.269	0.284
L-6	49	45.41	55.1	Wedge	0.72	0.46	0.495	0.53	0.341	0.363
L-7	44	44.31	72.3	Base plane	0.49	0.431	0.457	0.38	0.334	0.354
L-8	56	66.57	76.7	Flexural toppling	0.57	0.54	0.549	0.43	0.42	0.446

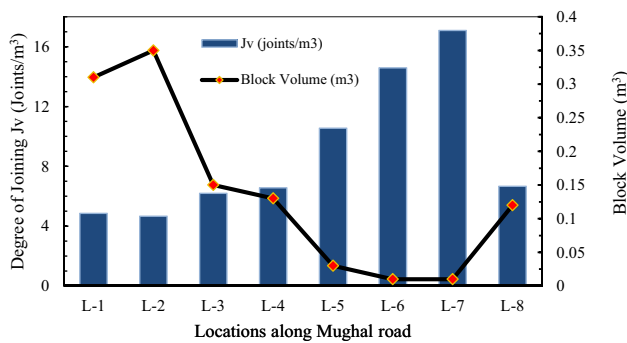


Fig. 9 Relation between Joint volume & Block volume along the study area

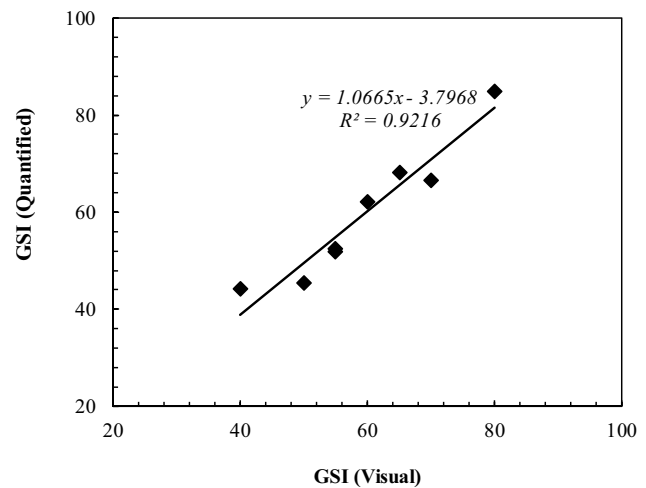


Fig. 11 Comparison of observed and calculated GSI

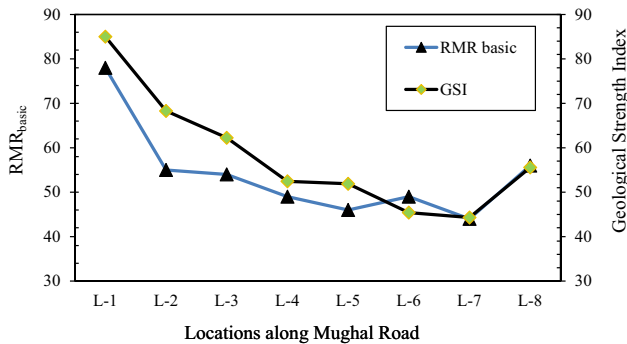


Fig. 10 Variation of RMR with GSI along the selected location of Mughal Road

defines its type of failure. The variation and relation of different failure types are presented in Fig. 14.

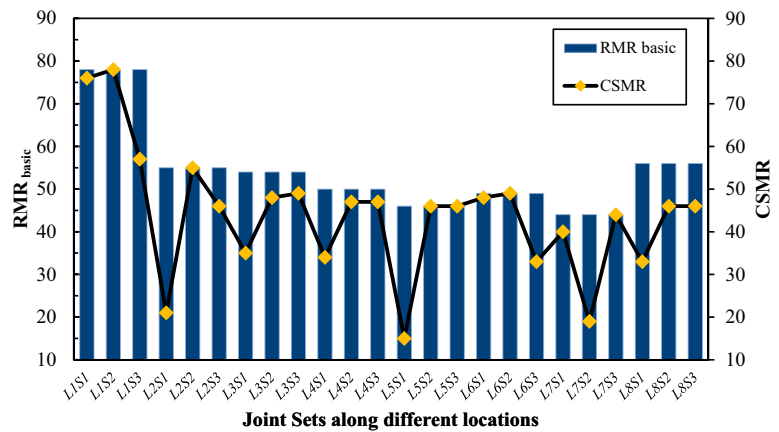
The more precise quantification of the most susceptible zone in these rock-cut slopes has been presented as the frequency variation of critical intersections of discontinuities (in %) and the slope face dips. The critical intersections are focused on a particular range of dip of slope face (70°–80°)

as is shown in Fig. 15. However, as seen from the variation chart, it can be inferred that some rock-cut slope dips show scattered variations of potential kinematic failures.

Limit Equilibrium and Pseudo-static Analysis

The LE and pseudo-static analyses for the selected slopes along the study area show FOS less than unity for all the slopes. The FOS has been calculated using both Mohr–Coulomb and Hoek–Brown models. The Mohr–Coulomb model was chosen as it is a widely used and practical choice for analysing rock slopes in the limit equilibrium. However, the Hoek–Brown model provides a more comprehensive and rock-specific approach, particularly for slopes with complex geological conditions. Hence, these soil models were adopted in this study for an accurate stability assessment. The LE analysis using different methods under static and pseudo-static loading indicates that the factor of safety varies from 0.4 to 0.8 under static loading and from 0.35 to 0.75 under pseudo-static

Fig. 12 Variation of SMR and RMR along the selected locations



Conclusion and Future Scope

Conclusion

Based on the tests and methods adopted, the following conclusions are drawn.

- (i) The RQD of the rock mass indicates the rock varies from 50 to 100 with small to medium-sized rock blocks and in this instance; the joint volume is as high as 17, which implies more susceptibility to failure.
- (ii) The uniaxial strength of the samples varies between 50 and 110 MPa. Such a vast diversity in the UCS results is attributed to the lithological features of the samples. The sample density, texture, and compactness along the study area varied drastically. The samples obtained at some locations had high surface voids, while others were too compact. It is worth mentioning here that the actual UCS of the rock mass varies from intact samples due to the presence of joints and discontinuities. Hence, the proper adjustments concerning joints as indicated by the GSI values were applied to arrive at the UCS of the rock mass.
- (iii) The RMR basic varies from 40 to 80, indicating fair to good rock mass.
- (iv) The SMR analysis shows that the slope mass varies from completely unstable to stable for different failure modes, with a probability of failure at some slopes as high as 0.9.
- (v) The kinematic analysis of these slopes indicates a variety of slope failures along different orientations. The overall critical intersections for different failure modes vary between 0 and 52%. The orientation of the joints along the study area defines its type of failure.

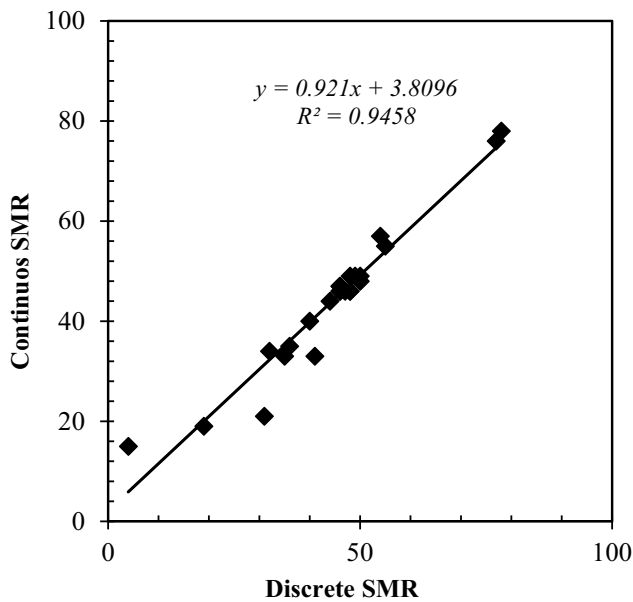


Fig. 13 Comparison of discrete and continuous SMR

loading. The low factor of safety is attributed to the randomly oriented joints and their persistence. Further, the lower FOS observed on the on-site slope is likely due to the severe slope conditions present, which may fail at any time. The variation of FOS as calculated from both the failure criteria is presented in Fig. 16. From the above comparison of FOS from two failure criteria, it can be inferred that Mohr–Coulomb Model for rock masses gives conservative results. This variation results due to the non-inclusion of discontinuity data of rock mass in the Mohr Coulomb model.

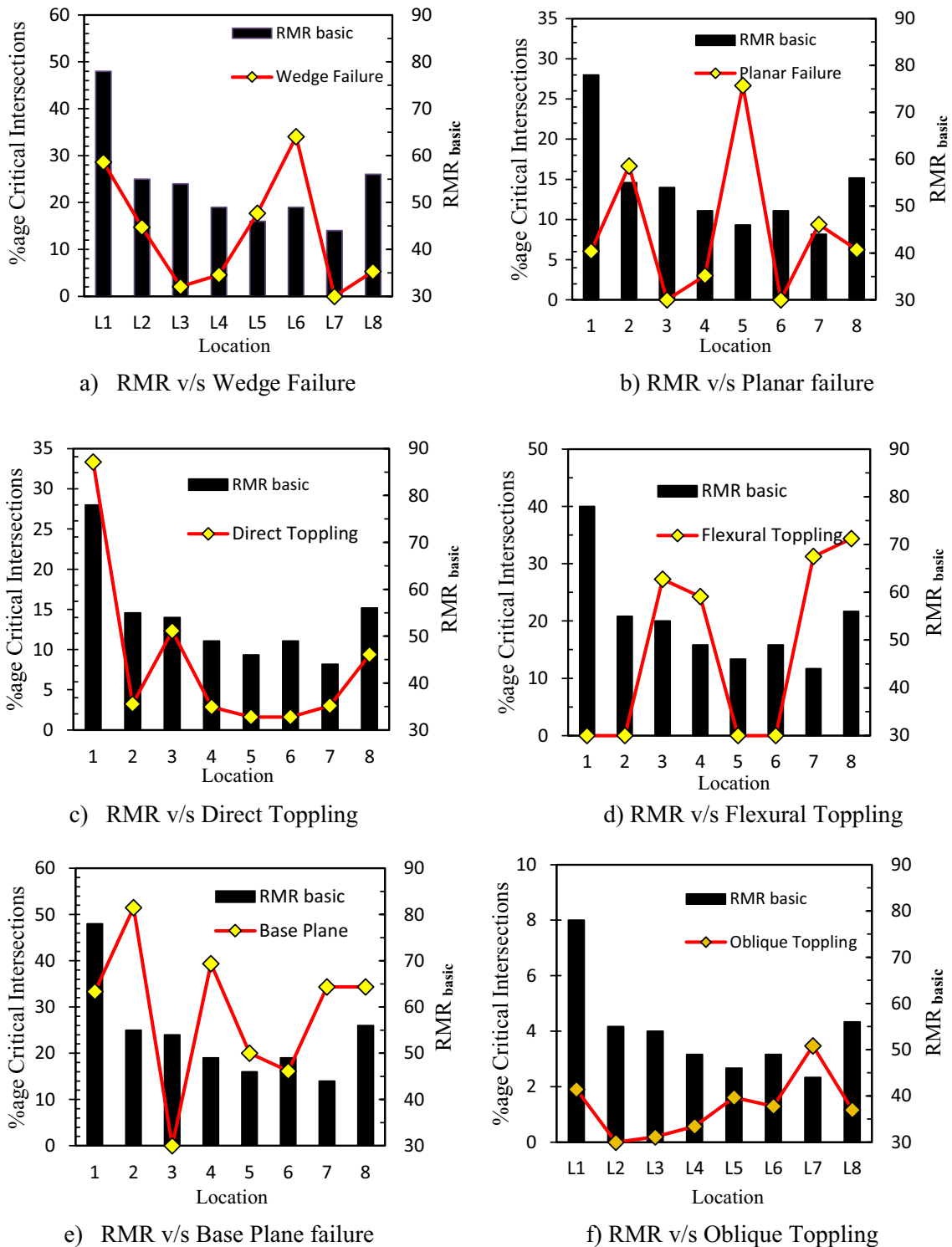


Fig. 14 Variation of failure modes with RMR along study sites

(vi) The LE analysis using different methods under static and pseudo-static loading indicates that the factor of safety varies from 0.4 to 0.8 under static loading while from 0.35 to 0.75 under pseudo-static loading.

The low factor of safety is attributed to the randomly oriented joints and their persistence. The alternate freeze and thaw, owing to the climate in the study, also plays an additional role in decreasing the resis-

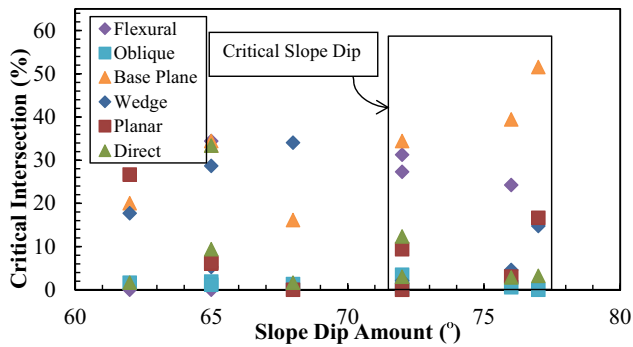


Fig. 15 Variation of failure potential with slope dip amount along the study area

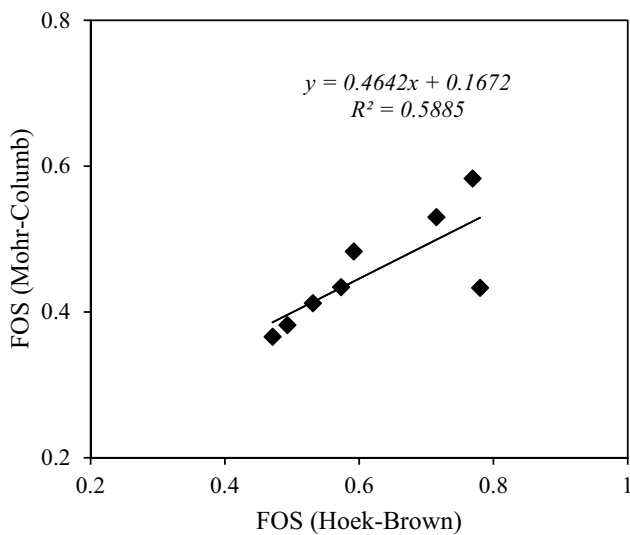


Fig. 16 Comparison of FOS from MC and HB Models

tive force. The heavy snow loads during the winters also weakened the slopes there.

Overall, the Rock Mass Quality (RQD) values, ranging from 50 to 100, signify a rock mass with a substantial joint presence, indicating heightened susceptibility to instability. This assessment is substantiated by the wide variability in Unconfined Compressive Strength (UCS) results, spanning 50 to 110 MPa, which can be attributed to varying sample properties. The Rock Mass Rating (RMR) values between 40 and 80 denote a rock mass ranging from fair to good quality. However, the Slope Mass Rating (SMR) analysis suggests that some slopes exhibit a high probability of failure (up to 90%). When considering the results of Limit Equilibrium (LE) analysis, the factor of safety ranges from 0.35 to 0.8 under static and pseudo-static loading conditions, indicating a lower level of stability. Together, these findings underscore the complex and

heterogeneous nature of the rock mass, emphasizing the need for thorough site-specific assessments, tailored engineering measures, and rigorous monitoring to ensure slope stability and mitigate potential risks effectively.

Limitations and Future Scope

Even though the present work was done with proper interest and in line with the standards set by pioneer workers, the limitations and hence future scope is discussed below:

- (i) *Survey Part*: Scanning the discontinuities was done using a scan-line survey which involves manual measurement and recording of the data. The main disadvantage is that a small or lesser distances are traversed in a given time. Hence to overcome this limitation, modern methods like LiDAR (Light Detection and Ranging) and Photogrammetry with automatic data acquisition and processing can be resorted to.
- (ii) *Investigation Part*: The GSI was used in conjunction with the Hoek Brown failure criterion to determine rock mass characteristics in this present. The Hoek–Brown and GSI failure criteria are both based on empirical charts and calculations. The capacity and precision of these methods are restricted. It is advised that rock mass characteristics be estimated using numerical modeling by integrating discontinuity geometry parameter estimations acquired from fracture mapping findings with intact rock and discontinuity properties established in the lab.
- (iii) *Numerical Analysis*: The slopes were analyzed in the Geo-Studio software and LE analysis was carried out using Hoek–Brown and Mohr–Coulomb failure criteria. Wu and Kulatilake [46] proposed a method for estimating rock mass characteristics that consider both intact rock and small discontinuities. They have developed the software 3DEC (3-Dimensional Distinct Element Code) for fracture mapping. However, analysis using 3DEC is not considered in the present study.

Acknowledgements The authors appreciate the financial support provided by the Science and Engineering Research Board, Department of Science and Technology, India (Grant No. EEQ/2021/001071 dated 14 March, 2022).

Data availability All the data is presented in the manuscript.

Declarations

Conflict of interest The authors have no competing interests to declare that are relevant to the content of this article.

References

- Hewitt K, Clague JJ, Deline P (2011) Catastrophic rock slope failures and mountain glaciers. In: Singh VP, Singh P, Haritashya T (eds) *Encyclopedia of Snow, Ice and Glaciers*. Springer, London, pp 113–126. https://doi.org/10.1007/978-90-481-2642-2_615
- Stead D, Eberhardt E (2013) Understanding the mechanics of large landslides. *Ital J Eng Geol Environ Book Ser* 6:85–112
- Guerra AJT, Fullen MA, Jorge MDCO, Bezerra JFR, Shokr MS (2017) Slope processes, mass movement and soil erosion: a review. *Pedosphere* 27(1):27–41
- Ansari T, Kainthola A, Singh KH, Singh TN, Sazid M (2021) Geotechnical and micro-structural characteristics of phyllite derived soil; implications for slope stability, Lesser Himalaya, Uttarakhand, India. *CATENA* 196:104906
- Shahnazari H, Chenari RJ, Fard MK, Heshmati S (2018) Stability evaluation of un-braced cuts. *Int J Civ Eng* 16:1361–1369
- Clague JJ, Stead D (2012) *Landslides: types, mechanisms and modeling*. Cambridge University Press, Cambridge
- Hearn GJ, Shakya NM (2017) Engineering challenges for sustainable road access in the Himalayas. *Q J Eng Geol Hydrogeol* 50(1):69–80
- Lee DH, Lai MH, Wu JH, Chi YY, Ko WT, Lee BL (2013) Slope management criteria for Alishan Highway based on database of heavy rainfall-induced slope failures. *Eng Geol* 162:97–107
- Latha GM, Garaga A (2010) Seismic stability analysis Himalayan rock slope. *Rock Mech Rock Eng* 43:831–843
- Singh R, Umrao RK, Singh TN (2017) Hill slope stability analysis using two and three dimensions analysis: a comparative study. *J Geol Soc India* 8:295–302
- Jing L, Hudson JA (2002) Numerical methods in rock mechanics. *Int J Rock Mech Min Sci* 39(4):409–427
- Pantelidis L (2009) Rock slope stability assessment through rock mass classification systems. *Int J Rock Mech Min Sci* 46(2):315–325
- Bieniawski ZT (1974) Engineering classification of jointed rock masses. *Discuss Pap Civ Eng Siviele Ingenieurswese* 12:335–343
- Bieniawski ZT (1973) Engineering classification of jointed rock masses. *Civ Eng Siviele Ingenieurswese* 12:335–343
- Hoek E, Brown ET (1997) Practical estimates of rock mass strength. *Int J Rock Mech Min Sci* 34:1165–1186
- Bar N, Barton N (2017) The Q-slope method for rock slope engineering. *Rock Mech Rock Eng* 50:3307–3322
- Romana MR (1993) A geomechanical classification for slopes: slope mass rating. *Comprehensive rock engineering. Rock testing and site characterization*, Pergamon, pp 575–600
- Hoek E, Carter TG, Diederichs MS (2013) Quantification of the geological strength index chart. In: 47th US rock mechanics/geomechanics symposium. OnePetro
- Palmström A (2001) Measurement and characterizations of rock mass jointing. *In-situ characterization of rocks*, pp 1–40
- Brown ET (1981) Rock characterization testing and monitoring. ISRM suggested methods. *Int J Rock Mech Min Sci Geomech Abstr* 18(6):109
- Russo A, Hormazabal E (2019) Correlations between various rock mass classification systems, including laubscher (MRMR), Bieniawski (RMR), Barton (Q) and Hoek and Marinos (GSI) Systems. In: *Geotechnical engineering in the XXI century: lessons learned and future challenges*. IOS Press, London, pp 2806–2815
- Tomás R, Delgado J, Serón JB (2007) Modification of slope mass rating (SMR) by continuous functions. *Int J Rock Mech Min Sci* 44(7):1062–1069
- Acharya B, Sarkar K, Singh AK, Chawla S (2020) Preliminary slope stability analysis and discontinuities driven susceptibility zonation along a crucial highway corridor in higher Himalaya, India. *J Mt Sci* 17:801–823
- Hammah RE, Yacoub T, Corkum B, Wibowo F, Curran JH (2007) Analysis of blocky rock slopes with finite element Shear Strength Reduction analysis. In: 1st Canada-US rock mechanics symposium. OnePetro
- Diederichs MS, Lato M, Hammah R, Quinn P (2007) Shear strength reduction (SSR) approach for slope stability analyses. In: 1st Canada-US rock mechanics symposium. OnePetro
- Shroder JF, Bishop MP (1998) Mass movement in the Himalaya: new insights and research directions. *Geomorphol* 26(1–3):13–35
- Siddique T, Mondal MEA, Pradhan SP, Salman M, Sohel M (2020) Geotechnical assessment of cut slopes in the landslide-prone Himalayas: rock mass characterization and simulation approach. *Nat Hazards* 104:413–435
- Anbalagan R (1992) Landslide hazard evaluation and zonation mapping in mountainous terrain. *Eng Geol* 32(4):269–277
- Jamir I, Gupta V, Kumar V, Thong GT (2017) Evaluation of potential surface instability using finite element method in Kharsali Village, Yamuna Valley, Northwest Himalaya. *J Mt Sci* 14(8):1666–1676
- Gansser A (2011) The geodynamic history of the Himalaya. *Zagros Hindu Kush Himal Geodyn Evol* 3:111–121
- Wakhloo S, Shah S (1968) A note on Baftiaz volcanics of Western Pir Panjal. *Publ Center Adv Study Goel Punjab Univ* 5:53–64
- Fultz B, Howe JM (2001) Diffraction and the X-ray powder diffractometer. In: *Transmission electron microscopy and diffractometry of materials*. Springer, Berlin
- IS 13365 (Part 1) (2010) Quantitative classification systems of rock mass—guidelines. Bureau of Indian Standards, New Delhi
- Smith JV (2015) A new approach to kinematic analysis of stress-induced structural slope instability. *Eng Geol* 1:56–59
- Goodman RE (1989) *Introduction to rock mechanic*. Wiley, London
- Hoek E, Bray JW, Boyd JM (1973) The stability of a rock slope containing a wedge resting on two intersecting discontinuities. *Quart J Eng Geol* 6(1):1–55
- Hoek E, Bray JW (1981) *Rock slope engineering revised*, 3rd edn. The Institution of Mining and Metallurgy, London
- Huang YPH (2014) Slope stability analysis by the limit equilibrium method: fundamentals and methods. *Am Soc Civ Eng*. <https://doi.org/10.1061/9780784412886>
- Rajhans P, Ekbote AG, Bhatt G (2022) Stability analysis of mine overburden dump and improvement by soil nailing. *Mater Today: Proc* 65:735–740
- Hoek E, Marinos P (2007) A brief history of the development of the Hoek–Brown failure criterion. *Soils and Rocks* 2(2):2–13
- Yang CW, Zhang JJ, Fu X, Zhu CB, Bi JW (2014) Improvement of pseudo-static method for slope stability analysis. *J Mt Sci* 11:625–633
- Metya S, Chaudhary N, Sharma KK (2021) Pseudo static stability analysis of rock slope using Patton’s shear criterion. *Int J Geo-Eng* 12:1–22
- Barton N, Lien R, Lunde J (1974) Engineering classification of rock masses for the design of tunnel support. *J Rock Mech* 6:4. <https://doi.org/10.1007/BF01239496>
- Romana M (1985) New adjustment ratings for application of bieniawski classification to slopes. In: *Int. Svm. on the role of rock mechanics, Zacatecas*, pp 49–53

45. Mohamad ET, Abad S (2011) Assessment on blasting-induced rock slope instability at Johor, Malaysia. *Electron J Geo Eng* 16:357–374
46. Wu Q, Kulatilake PHSW (2012) REV and its properties on fracture system and mechanical properties, and an orthotropic constitutive model for a jointed rock mass in a dam site in China. *Comput Geotech* 43:124–142

Springer Nature or its licensor (e.g. a society or other partner) holds exclusive rights to this article under a publishing agreement with the author(s) or other rightsholder(s); author self-archiving of the accepted manuscript version of this article is solely governed by the terms of such publishing agreement and applicable law.

Publisher's Note Springer Nature remains neutral with regard to jurisdictional claims in published maps and institutional affiliations.